THE JOURNAL OF PHYSICAL CHEMISTRY C

Article

Cite This: J. Phys. Chem. C 2017, 121, 27511−27520

pubs.acs.org/JPCC

Growth of Porous Anodic Alumina on Low-Index Surfaces of Al Single Crystals

Ilya V. Roslyakov,[†,‡] Dmitry S. Koshkodaev,[‡] Andrei A. Eliseev,[†,‡] Daniel Hermida-Merino,[§] Vladimir K. Ivanov,[∥,⊥] Andrei V. Petukhov,[#,∇] and Kirill S. Napolskii*[,†,‡]

[†]Department of Chemistry and [‡]Department of Materials Science, Lomonosov Moscow State University, Moscow 119991, Russia

[§]DUBBLE CRG ESRF BM26, F-38043 Grenoble Cedex, France

[∥]Kurnakov Institute of General and Inorganic Chemistry, RAS, Moscow 119991, Russia

[⊥]Department of Chemistry, National Research Tomsk State University, Tomsk 634050, Russia

[#]van 't Hoff Laboratory for Physical and Colloid Chemistry, Debye Institute for Nanomaterials Science, Utrecht University, 3508 TB Utrecht, The Netherlands

[∇]Laboratory of Physical Chemistry, Department of Chemical Engineering and Chemistry, Eindhoven University of Technology, Eindhoven 5600 MB, The Netherlands

Supporting Information

ABSTRACT: The pseudoepitaxial growth of amorphous anodic alumina with ordered porous structure within single crystal grains of aluminum substrates is an amazing feature of the self-organization process, which occurs during anodization. Here, we used single crystal Al(100), Al(110), and Al(111) substrates to inspect the effect of aluminum crystallography on anodization rates and the morphology of the resulting alumina films grown under different anodization conditions. The difference in the kinetics of porous film growth on various substrates is described in terms of the activation barrier of aluminum atom release from the metal surface to the oxide layer. Scanning electron microscopy and small-angle X-ray scattering are applied for quantitative characterization of different kinds of ordering in anodic alumina films. The highest number of straight channels was found in porous anodic alumina grown on Al(100) substrates, whereas Al(111) was proved to induce the best orientational order in anodic alumina with the formation of the single-domain-like structures. Based on the obtained results, possible pathways for crystallographic control of the anodic alumina porous structure for different practical applications are discussed.

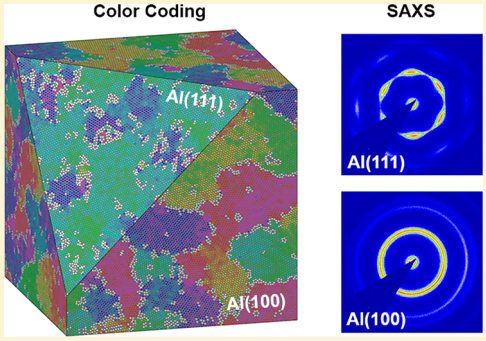

INTRODUCTION

Anodization of aluminum in acidic media is known as a facile tool for the formation of porous films with uniform vertically aligned channels. Pore diameter, interpore distance, and thickness of anodic aluminum oxide (AAO) layer can be easily tuned in wide range by varying experimental conditions.[1,2] A unique AAO geometry with extremely high pore density (ca. 10^{10} to 10^{11} cm^{-2}) and narrow pore size distribution opens great opportunities for using porous anodic alumina films in different areas of science and technology.[3,4] In particular, highly efficient membranes for gas separation,[5,6] metal and semiconductor nanowires for catalytic applications,[7,8] data storage,[9,10] microelectronics,[11] large-scale photonic crystals for manipulation of light,[12,13] highly efficient capacitors,[14,15] and gas sensors with ultralow power consumption[16−18] have been prepared based on anodic alumina.

The maximum performance of AAO (e.g., well-defined pore size and interpore distance, enhanced thermal stability, and permeability) is expectedly observed for the oxide films possessing a highly ordered two-dimensional hexagonal arrangement of pores,[19,20] which forms solely under strict anodization conditions as dictated by the electrode reaction kinetics.[21]

To characterize pore arrangement in the AAO structure quantitatively, three kinds of ordering should be considered:

(i) transverse (in-plane) positional order correlating to the dispersion of interpore distances;
(ii) transverse (in-plane) orientational order related to the preservation of the in-plane orientations of the hexagons formed by neighboring channels, which determines the mosaicity of porous structure;
(iii) longitudinal (out-of-plane) orientational order defining how well the direction of pore growth is maintained across the film.

Received: October 9, 2017
Revised: November 17, 2017
Published: November 22, 2017

DOI: 10.1021/acs.jpcc.7b09998
J. Phys. Chem. C 2017, 121, 27511−27520

In the past decade, the ability to control the morphology of AAO films by choosing the proper crystallographic orientation of the Al substrate has been successfully demonstrated. The first results in this field were obtained in 2007, when aluminum with the coarse-grained microstructure was stated as a requirement for extending transverse orientational correlations in the AAO structure to a centimeter scale.[22] Later a correlation between the size of the regions with perfect hexagonal pore ordering (the size of domains) in the AAO porous structure and the crystallographic orientation of the Al substrate has been shown: the largest mean domain size and, as a consequence, the best transverse positional order have been observed for aluminum foils with (100) texture.[23] In 2011, the structure of anodic alumina formed in sulfuric acid on the surface of the single crystals of aluminum with (111), (110), and (100) orientations was analyzed.[24] According to scanning electron microscopy (SEM) measurements the smallest fraction of defects (dislocations and high- and low-angle grain boundaries) has been found for the Al(100) substrate. Obtained results have been described in terms of minimizing the AAO/Al interface energy.

According to previously reported data,[25] AAO with the best transverse positional order of the pores is formed on (100)-oriented Al grains, whereas pore arrangement in the films grown on Al(110) do not show any resemblance to a hexagonal pattern. A theoretical description of this phenomenon has been performed by numerical simulations of the pore growth process involving different ratios of the formation of free and bound forms of Al^{3+} ions at the Al/AAO interface.[26] An alternative explanation proposed for the influence of the crystallographic orientation of the Al substrate on the ordering of the amorphous AAO porous structure involves the anisotropy of aluminum oxidation rates, which governs long-range transverse orientational pore ordering.[27] Indeed, the mosaicity of the porous structure was found to be minimal in the case of AAO grown on Al(111) faces with 6-fold symmetry, whereas in the case of the 4-fold symmetry Al(100) crystal two equivalent options for the arrangement of a hexagonal lattice of pores were shown. To summarize, there are several contradictory theories and experimental results concerning the influence of the Al crystallographic orientation on the morphology of AAO porous films. At the same time, any reliable proofs concerning optimal substrate symmetry for the best hexagonal arrangement of pores in AAO films are still absent.

Earlier we proposed small-angle X-ray scattering (SAXS) as a unique tool for the quantitative characterization of pore arrangement in anodic alumina across the whole film thickness.[28] This technique provides exclusive information on pore growth direction as well as on pores arrangement across the film. The inclination of the channels from the surface normal has been disclosed by SAXS.[29,30] Moreover, the correlation between the longitudinal alignment of pores and the transverse orientational order in AAO has been revealed by small-angle X-ray diffraction experiments on anodic alumina grown on Al(100) single crystals substrates with a number of vicinal facets.[30]

Here, SAXS technique in combination with the statistical analysis of SEM images is applied for the comparative study of the 3D porous structure of AAO films grown on the low-index surfaces of aluminum single crystals. To establish the anisotropy of anodic oxidation rates on different aluminum faces oxidation kinetics was also analyzed.

EXPERIMENTAL SECTION

Three sets of the aluminum single-crystal substrates (99.9999%, 2 mm thick, mechanically polished to a mirror finish) with the (100), (110), and (111) orientations were purchased from MESCREL.[31] Anodization of Al single crystals was carried out in the two-electrode electrochemical cell using a DC power supply Agilent N5751A. The electrolyte was cooled to 1−2 °C by a Huber K6 chiller and was pumped through the cell by a Heidolph 5006 peristaltic pump. The distance between the aluminum anode and a Pt wire ring that served as a cathode was 8 cm. The anodization area was restricted by a Viton O-ring with an internal diameter of 12 mm. Anodic alumina films were obtained in either mild or hard anodization regimes, in which the electrode reaction kinetics is limited by the migration of ions in the barrier layer and by the diffusion of ionic species in solution, respectively.[21] To achieve better pore ordering, in the case of the electrochemical oxidation of aluminum in 0.3 M sulfuric acid at 25 V and in 0.3 M oxalic acid at 40 V (mild anodization regimes) a two step anodization procedure was applied.[32] After the first anodization step, the porous oxide layer was selectively etched away in an aqueous solution containing 0.2 M CrO_3 and 0.5 M H_3PO_4 at 70 °C for 30 min. The second anodization step was performed under the same conditions as the first one. The electrochemical oxidation was terminated when the charge reached 105 and 210 C at the first and second step, respectively. These charge limits correspond to the thickness of oxide layer of ca. 50 and 100 μm, respectively.

Hard anodization of aluminum was carried out in 0.3 M oxalic acid at 120, 130, and 140 V. At the initial stage, the voltage was kept constant at 40 V for 30 min, and then it was increased with the rate of 0.5 V s^{-1} to the target value. The total thickness of protective and transitional layers did not exceed 9 μm. Anodization was terminated when the electric charge reached 260 C. This charge limit corresponds to the formation of ca. 130 μm thick AAO layer.

High-resolution small-angle X-ray scattering was used for the quantitative characterization of the ordering degree of porous AAO films formed on various facets of aluminum single crystals. Samples were placed on the translation/rotation stage to allow careful orientation around the horizontal and vertical axes orthogonal to the beam. To minimize absorption of the X-rays, Al substrates were partially dissolved in an aqueous solution containing 0.5 M $CuCl_2$ and 1.4 M HCl at room temperature. The diffraction experiments were performed at the beamline BM26B "DUBBLE"[33] of the European Synchrotron Radiation Facility in Grenoble (France) using a micro-radian X-ray diffraction setup.[34−36] A 13 keV X-ray beam with wavelength (λ) of 0.95 Å, bandpass ($\Delta\lambda/\lambda$) of 2×10^{-4}, and a footprint of 0.5 mm × 0.5 mm at the sample was used. The beam was focused by a set of beryllium compound refractive lenses[37,38] installed just in front of the sample. The lenses focused the beam at the phosphor screen of a 2D CCD detector (Photonic Science, 4008 × 2672 pixels of 22 μm × 22 μm). The detector was installed 7 m from the sample position.

Characterization of the crystallographic orientation of the single-crystal substrates and the morphology of the AAO porous films was carried out using a field-emission scanning electron microscope NVision 40 (Carl Zeiss) equipped with a Nordlys II(S) EBSD detector (Oxford Instruments). SEM images of the bottom part of the oxide film after removing a barrier layer in 5 wt % H_3PO_4 at 60 °C were used for the

DOI: 10.1021/acs.jpcc.7b09998
J. Phys. Chem. C 2017, 121, 27511−27520

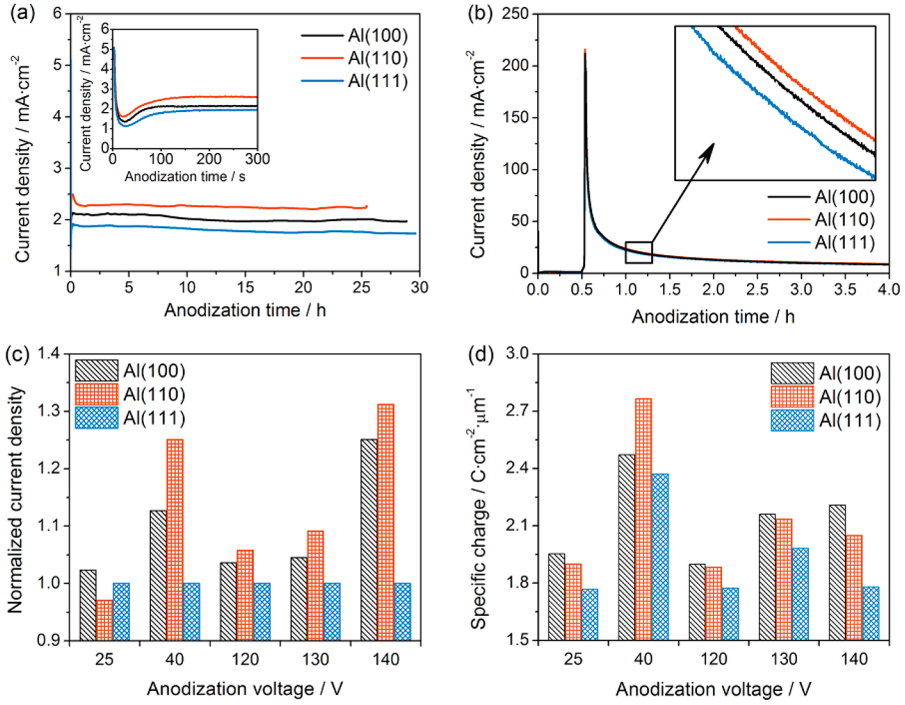

Figure 1. Kinetics of the anodization of Al single-crystal substrates with low-index surfaces. Current density−time (j−t) transients recorded during anodic oxidation in 0.3 M oxalic acid at (a) 40 V (curves for second anodization step are presented) and (b) 120 V. The insets present an initial stage (panel a) and random part (panel b) of the corresponding $j(t)$ curves. Panel c shows the ratios of average current density under certain anodization conditions (25 V in 0.3 M sulfuric acid; 40, 120, 130, and 140 V in 0.3 M oxalic acid) to average current density on Al(111). The currents were averaged over the entire anodization process. Specific charge values for different anodization conditions are presented in panel d.

analysis of the degree of pore ordering. Before investigation the samples were covered with a thin conductive layer of chromium using a Q150T ES sputter coater (Quorum Technologies). Statistical analysis of the SEM images was performed using a color-coding procedure for the examination of the in-plane orientational order and using a spreading algorithm for the determination of domain size distribution.[39] The statistical distribution of the number of the nearest neighbors around the considered pore was obtained by the Voronoi algorithm[40] using the ImageJ program[41] and self-developed software.[42]

RESULTS AND DISCUSSION

Anodization Kinetics. Typical current density−time (j−t) transients recorded in mild and hard anodization regimes are presented in Figure 1a,b, respectively. In 0.3 M oxalic acid at 40 V, the current density keeps constant during the entire anodization process. Contrary, at 120 V j decreases as $1/L$, where L is the thickness of the porous oxide layer. The difference is caused by the different nature of current-limiting stages in mild and hard anodization regimes.[21]

Comparing $j(t)$ curves at a certain voltage, a notable change in current density can be clearly seen for the anodization of Al single crystals with various crystallographic orientations. A decrease of more than 10% in current density is observed in the sequence of Al(110) − Al(100) − Al(111) in the case of anodization in 0.3 M oxalic acid at 40 V (Figure 1a). The same behavior is demonstrated in the hard anodization regime (Figure 1b,c): the current density increases in going from Al(111) to Al(100) and from Al(100) to Al(110).

Given the fact that all anodization parameters (e.g., temperature of electrolyte, rate of its agitation, anodization voltage, and sample area) were precisely controlled, that allows us to keep them exactly the same during electrochemical oxidation of various facets of Al single crystals, we can conclude that the difference in recorded current density is caused solely by the crystallographic orientation of the Al substrate. The observed behavior is in a good agreement with the reactivity of the low-index Al surfaces, as predicted by Periodic Bond Chain theory.[43,44]

The difference in oxidation rates can be analyzed quantitatively in terms of activation-controlled nature of the anodization process. Several stages of the anodic oxidation reaction were elucidated earlier including aluminum atom oxidation and its release from metal to oxide layer, transport of aluminum ion through a barrier layer, and ion transfer across the metal oxide/electrolyte interface producing a solvated ion.[2,45]

Taking account of the experimentally observed dependence of current density on the crystallographic orientation of the aluminum substrate, it is logical to assume that ion transfer across the metal/metal oxide interface has a strong influence on the kinetics of aluminum anodization. According to the Cabrera-Mott theory, describing the limiting case, when ion transfer across the metal/metal oxide interface is a rate-determining step, current density under high-field conditions could be written as

$$j_{hkl} = n_{hkl}\nu_{hkl}z \exp[-(W - zaE)/kT] \quad (1)$$

where n_{hkl} is the aluminum atomic density on the (hkl) facet, ν_{hkl} is the attempt frequency of a surface metal atom on the (hkl) facet, z is the charge on the mobile ion, W is the activation energy, a is the distance from the positions of minimum to the maximum potential energy, E is the electric

DOI: 10.1021/acs.jpcc.7b09998
J. Phys. Chem. C 2017, 121, 27511−27520

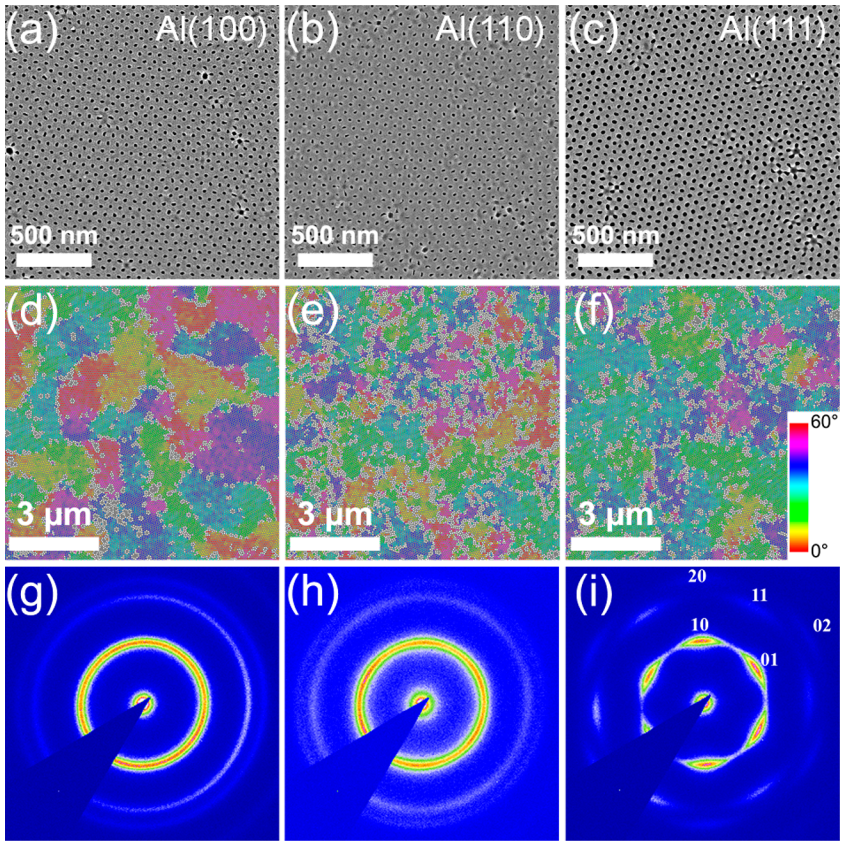

Figure 2. Morphology of the anodic alumina films formed on aluminum low-index single-crystal surfaces in 0.3 M sulfuric acid at 25 V by two-step anodization. (a–c) High magnification SEM images. (d–f) Low magnification SEM images subjected to the color coding procedure. Color indicates an average angle to the nearest neighbors of the considered pore. Pores having no apparent hexagonal coordination are marked white. (g–i) Small-angle diffraction patterns recorded for anodic alumina films under normal incident X-ray beam. *hk* indices for Bragg reflections are given (i).

field strength, k is Boltzmann constant, and T is absolute temperature.

We do not also exclude the possibility of the limitation of the rate of anodic oxidation by ion transfer through the barrier oxide layer (Verwey theory) or by ion transfer across the metal oxide/electrolyte interface. For these cases the difference in current density can appear due to the difference in the thickness of the barrier oxide layer formed on substrates with various crystallographic orientations. However, the mathematical form of the equations for current density does not changes principally from eq 1, while substituting atomic density and vibration frequencies of the metal/oxide interface to the parameters of bulk oxide or oxide/electrolyte interface.

We stress that absolute values of atom release energies are strongly dependent on absolute temperatures at aluminum/oxide interface and can hardly be obtained from the experiments. Thus, we extracted the difference in activation barriers for different substrates from current densities ratio neglecting the temperature difference during anodization:

$$\frac{j_{hk0}}{j_{111}} = \frac{n_{hk0}\nu_{hk0}}{n_{111}\nu_{111}}\exp[-(W_{hk0} - W_{111})/kT] \quad (2)$$

Experimental phonon frequencies for the corresponding k-points were used as attempt frequencies[46] (see the Supporting Information, Table S1). Calculations by eq 2 reveal a slight difference in experimental activation barriers of 15–20 meV, and those are believed to correspond aluminum atom release energies from the metal surface to the oxide layer. Unfortunately, we failed to find either experimental or theoretical values of barrier energies for anodic oxidation of different faces in the literature to reveal reaction limiting stage. Several estimates were used to compare the oxidation rates ratio for aluminum faces, all resulting in the same tendency of $j_{Al(110)} > j_{Al(100)} > j_{Al(111)}$ (see the Supporting Information, Table S1). Notably the absolute values of the activation energies for aluminum anodization in dissolving electrolytes are 1 order of magnitude higher, rated in the order of ∼0.5 eV according to our estimates (see the Supporting Information) and ranged from 0.5 to 0.9 eV in the literature.[47,48] Despite the rather small relative variation of the activation barriers of $\sim kT$ for different aluminum faces, that is enough to affect the growth of the dominant AAO structure. It implies the impact of substrate crystallography on organization of porous alumina.

The crystallographic orientation of the aluminum substrate also affects the kinetics of pore nucleation. The minima of the current density corresponding to the nucleation of the pores,[49,50] which is registered at ∼30 s in 0.3 M oxalic acid at 40 V, shift to the longer times in the sequence of Al(110) − Al(100) − Al(111) (see inset in Figure 1a). A similar behavior was observed earlier for anodic titania films on polycrystalline Ti foils:[51] pore nucleation and growth were retarded when the close-packed (0001) plane with high atomic density was parallel to the Ti surface.

The experimental values of specific charge (q) spent for growing 1 μm of AAO film vary from 1.7 to 2.8 C cm^{-2} μm^{-1} depending on anodization conditions (Figure 1d). The general trend is that the fraction of electrochemically oxidized metal

DOI: 10.1021/acs.jpcc.7b09998
J. Phys. Chem. C 2017, 121, 27511–27520

atoms retained in the film increases with anodic current density. A measurable effect of substrate crystallography on anodic film formation was also revealed while comparing the thickness of the films formed on different substrates under the same anodization conditions. The specific charge varies in the following manner: $q_{Al(100)} \approx q_{Al(110)} > q_{Al(111)}$ (Figure 1d). Taking account of the current densities observed on different crystal faces (Figure 1c), the sequence of q values for low-index surfaces is opposite to the general trend discussed above. This allows us to ascribe the effect to the anisotropy of the expansion of material during aluminum oxidation on the metal/oxide interface having a maximum in the [111] direction.

Transverse Orientational Order. Typical SEM images of porous anodic alumina films grown onto (100), (110), and (111) low-index surfaces of Al single crystals are presented in Figure 2a–c, respectively. At first glance, all of the images look identical: pores are arranged into a two-dimensional hexagonal structure within micron-scale ordered regions. Below, these regions will be referred to as "domains".

To analyze pore ordering quantitatively, a color cording procedure[27,39] was applied for the SEM images recorded at low magnification. At least, 20 SEM images each containing of about 10^4 pores were evaluated for each sample. The typical patterns are shown in Figure 2d–f, where the average in-plane orientation of the nearest six neighbors to the given pore is coded by its color (see color scale on the inset in Figure 2f), whereas defects are marked white. It can be clearly seen that a large number of pores (20.1 ± 1.1%) without apparent hexagonal coordination are present in AAO on the Al(110) substrate (Figure 2e). The same parameter for the Al(100) substrate (Figure 2d) equals to 9.5 ± 0.9%. In this case, defects are concentrated on the high-angle domain boundaries rather than inside domains. On the Al(111) substrate (Figure 2f) almost all domains possess a similar in-plane orientation. Point defects (13.5 ± 0.6% of total number of pores) are located inside large domains, which are connected via low-angle boundaries.

According to color coding procedure (Figure 2d–f) domains with all possible orientations are present in the structure of AAO independently of the crystallographic orientation of the substrate. However, a significant change in the intensity distribution can be clearly seen on SAXS patterns (Figure 2g–i). In the case of the normal incidence of X-rays onto the AAO film formed on the Al(100) surface, several rings with the uniform distribution of intensity are observed. The absence of the preferred in-plane orientation originates from the incompatibility of the 4-fold crystallographic symmetry of the underlying metal crystal and the hexagonal symmetry of the perfect AAO structure. As a result, the absolute equivalence of the porous domains, which are misoriented on 90°, is observed. On the contrary, the Al(111) substrate with 6-fold symmetry exhibits the most strong orientation preferences, which manifest themselves by a distinct decrease in the mosaicity of the hexagonal porous structure. It is worth noting that the [110] direction, which is characterized by the highest atomic packing density in *fcc* crystals, acts here as a bearing axis for alignment of pore rows in plane of the oxide film. In the case of the Al(110) substrate, six broad maxima represent an intermediate degree of the in-plane orientational ordering of the pores.

The azimuthal intensity distributions for the first-order Bragg reflections obtained from the diffraction patterns are presented in Figure 3a. Similar structural information extracted from

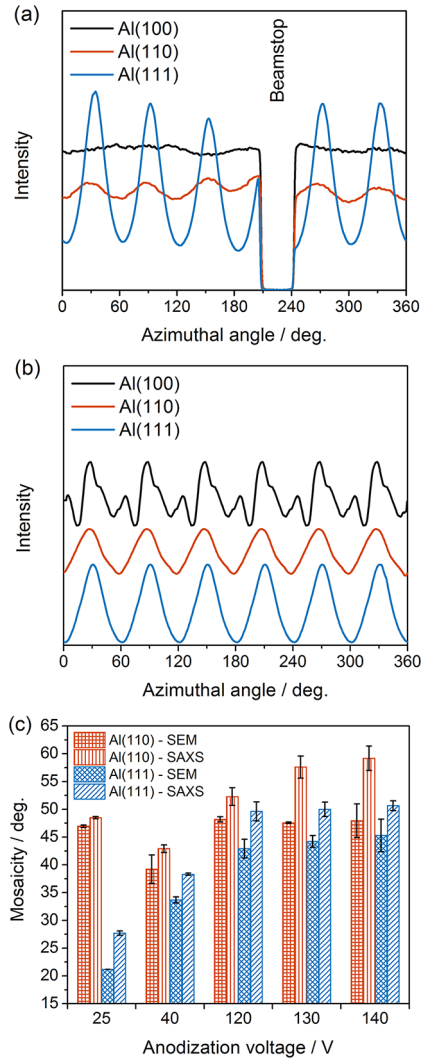

Figure 3. (a) Azimuthal intensity distribution profiles for the first-order Bragg reflections on SAXS patterns. (b) Transverse orientational correlations in the AAO structure according to statistical analysis of SEM images. Anodic oxide films were grown on the Al single-crystal substrates with different low-index surfaces by a two-step procedure in 0.3 M sulfuric acid at 25 V. (c) Mosaicity of porous oxide films formed on different low-index surfaces of Al single crystals under different anodization conditions (25 V in 0.3 M sulfuric acid; 40, 120, 130, and 140 V in 0.3 M oxalic acid).

statistical orientation analysis of SEM images is shown in Figure 3b. We point out the presence of 12-fold modulation of the occurrence frequency on Al(100) with the intermaxima intervals of ca. 30°, which confirms the presence of two preferential orientations of domains in the AAO porous structure.

Figure 3c summarizes the mosaicity values (the full width on the half-maximum of the peaks in the azimuthal profiles) of the porous structures grown on the different low-index single-crystal surfaces of Al under different anodization conditions. The highest in-plane orientational order (the lowest mosaicity) of AAO is always realized on Al(111) substrates. We should note that the mosaicity values deduced from the SAXS patterns and from the statistical analysis of SEM images via the color-coding procedure are close to each other. Nevertheless, the mosaicity obtained from SEM is lower than that obtained from SAXS because the color-coding algorithm ignores point defects

DOI: 10.1021/acs.jpcc.7b09998
J. Phys. Chem. C 2017, 121, 27511–27520

in the AAO structure. Moreover, SEM results represent ordering parameters only from the most ordered bottom side of the AAO surface, whereas SAXS data gives us average values from the whole film structure.

The domain size distribution in AAO films obtained in 0.3 M oxalic acid at 40 V is presented in Figure 4. The highest amount

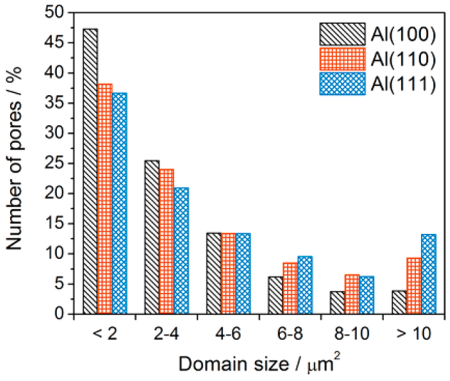

Figure 4. Distribution of the pores over the domains with different sizes. Two-step anodization of different low-index surfaces of Al single crystals was carried out in 0.3 M oxalic acid at 40 V.

of small domains is observed for AAO on Al(100) surface, where the equivalence of two specific directions for alignment of the rows of pores exist. It should be noted that ordered areas of more than 10 μm^2 in size are nearly absent on Al(100) substrate. On the contrary, aluminum with one bearing axis for the pore alignment (e.g., Al(110) and Al(111)) is prone to formation of the single-domain-like porous structures. In the case of Al(111) the large ordered areas of more than 10 μm^2 in size include of about 10% of pores. Nevertheless, we should stress that small domains prevail in the structure of all studied samples.

Transverse Positional Order. The in-plane positional order determines the dispersion of interpore distances and is characterized by the radial width of the diffraction maxima. The small-angle diffraction patterns (Figure 2) demonstrate several orders of the Bragg reflections for AAO films grown onto all low-index surfaces of Al single crystals. The radial profiles of the scattered intensity $I(q)$ demonstrate three clear maxima with a ratio of peak positions of $1:\sqrt{3}:2$ (Figure 5a). We stress that the shape of the $I(q)$ curves is very similar for all single-crystal substrates. In particular, in the case of the Al(110) substrate we did not observe the formation of the fully disordered porous structure without domains as it was reported before.[25]

Quantitative characterization of the in-plane positional order was carried out according to the proposed earlier protocol of the SAXS data treatment.[28] Briefly, the $I(q)$ curves were normalized on the form factor of pores $F(q)$, which was calculated based on the geometric parameters of the AAO structure (diameter and length of the channels, pore-size distribution, and orientation distribution functions). Approximation of the structure factor $S(q) = I(q)/F(q)$ by a sum of the Lorentz profiles yields the radial widths of the diffraction maxima. The average domain size in terms of the amount of structure periods was roughly estimated from the ratio of the position of the first-order Bragg peak (q_{10}) to the peak width (δq_{10}).

According to Figure 5b, the two-step technique in the mild anodization regime yields the formation of highly ordered porous structures with the average domain size of about 10 structure periods. It is worth noting that this value can be increased slightly by an increase in duration or number of anodization steps. In the hard anodization regime, the ratio $q_{10}/\delta q_{10}$ decreases by more than 1.5 times. The influence of the crystallographic orientation of the substrate on in-plane positional order is small enough, and systematic change in the $q_{10}/\delta q_{10}$ ratio for single-crystal substrates with various orientations is not observed.

Longitudinal Orientational Order. Rocking curves, which represent the intensity for the 10 Bragg reflections as a function of sample orientation (for more details please refer to our recent papers),[28,30] were used for the evaluation of longitudinal alignment of AAO channels. Obtained dependences (Figure 6a) reflect the orientational distribution of pores along the growth direction. A narrow maximum with a center at normal incidence of the X-ray beam to AAO film indicates the uniform growth of the AAO channels, which are parallel to each other and orthogonal to the film surface, for all low-index surfaces of single crystal Al studied in this work. It is worth noting that for the random crystallographic orientation of the Al facet the inclination of the pore growth direction from surface normal by several degrees was observed.[29]

The full width at half-maximum (fwhm) values of the rocking curves for AAO films formed under different conditions are given in Figure 6b. In the mild anodization regimes, the

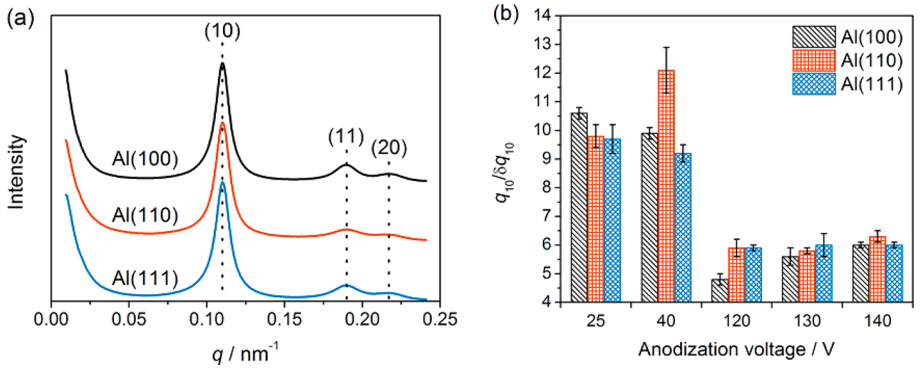

Figure 5. (a) Radial profiles $I(q)$ of the scattering intensity distributions obtained from the SAXS experiments at normal incidence of the X-ray beam to the AAO film surface. The *hk* indices are indicated. Two-step anodization was carried out in 0.3 M sulfuric acid at 25 V. (b) Average domain size in terms of an amount of structure periods for the alumina films grown on the Al single-crystal substrates with different low-index surfaces under different anodization conditions.

DOI: 10.1021/acs.jpcc.7b09998
J. Phys. Chem. C 2017, 121, 27511−27520

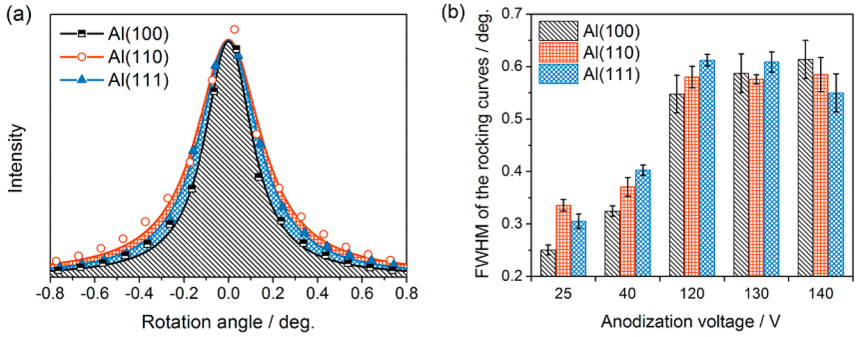

Figure 6. (a) Rocking curves for 10 Bragg reflections recorded for the anodic alumina films grown on the different low-index surfaces of single-crystal aluminum by two-step anodization in 0.3 M sulfuric acid at 25 V. The lines show the results of the Lorentz fit. (b) The full width at half-maximum (fwhm) of the rocking curves according to the Lorentz fit of the experimental data obtained for AAO films formed at 25 V in 0.3 M sulfuric acid and at 40, 120, 130, and 140 V in 0.3 M oxalic acid electrolyte.

alumina films on the Al(100) substrates demonstrate the smallest fwhm values of the rocking curves. Most probably, it is caused by parallel arrangement of surface normal that coincides with the direction of ion migration in the barrier layer and stable (100) crystallographic planes that act as guides for pore growth,[30] because the crossing of them by pores is accompanied by atoms release from the dense atomic planes and, hence, is energetically unfavorable. Contrariwise, in the case of Al(111), dense atomic planes orthogonal to the AAO film surface are absent. The angles of the substrate surface with (111) and (100) planes are 70.5° and 54.7°, respectively. Crossing of these planes by pores leads to the disturbance of longitudinal orientation, and as a result, the fwhm values of the rocking curves for porous films on Al(111) are systematically higher than for oxide layers on Al(100).

Switching to hard-anodization regimes (120−140 V in 0.3 M oxalic acid) significantly increases the width of the rocking curves (Figure 6b). First, it is caused by the presence of a disordered porous layer formed during the voltage increase stage. In the case of the voltage sweep rate of 0.5 V s^{-1}, this layer is about 9 μm thick and exhibits a very high dispersion of the growth direction of pores with a fwhm of the rocking curve of about 5°.[52] Second, the gradual increase in interpore distance even at a constant voltage stage also occurs,[53] because of gradual decrease in temperature at the pore bases. This structural feature of AAO formed in hard anodization regimes results in broadening of the rocking curve as well. Consequently, rocking curves are broader in the case of the hard-anodization regime in comparison with the mild ones. It is worth noting that the noticeable difference in fwhm of the rocking curves for the Al single-crystal substrates with different symmetry mostly disappears in the hard anodization regime (Figure 6b).

Crystallographic Control of the Porous Structure. The combination of small-angle X-ray scattering and scanning electron microscopy allows us to disclose the following key features of the morphology of porous anodic alumina layers formed on low-index Al surfaces (see also the quantitative values of different parameters of pore ordering in Table 1).

The in-plane orientational order and mosaicity of the AAO porous structure is completely predetermined by the symmetry of the anodized Al surface. The Al(111) substrate with the 6-fold rotation axis normal to the surface is prone to formation of the hexagonally ordered areas on a large scale, whereas the 4-fold symmetry of the Al(100) substrate leads to a large number of completely misoriented small domains. The in-plane orientational order in anodic alumina films formed onto Al(111) is restricted only by the size of the substrate.

The in-plane positional order of AAO channels is nearly independent of the substrate symmetry. Nevertheless, on the microscopic scale the distribution of the defects in the AAO structure is completely different for various orientations of the Al substrate. In the case of the Al(100) substrate the defects are concentrated on the high-angle domain boundaries, whereas in AAO formed on Al(111) the pores without a hexagonal neighborhood are located inside large domains, which are connected via low-angle boundaries.

The highest degree of longitudinal orientational order and the smallest inclination of the channels from the surface normal is observed for the Al(100) single-crystal substrates, when the grow direction of the pores is parallel to the stable crystallographic planes with dense atom packing.

Based on our findings we can conclude that anodic alumina porous films formed on Al(100) substrates are appropriate for the formation of high-quality AAO membranes[19] and templates[20] with mostly straight channels. Al(111) substrates are prone to the formation of single-domain-like structures, which are needed for the preparation of 2D photonic crystals, for fabrication of calibration gratings for AFM tips,[54,55] and for creation of patterned magnetic recording media.[9] Aluminum with a (110) crystallographic orientation should be avoided in preparation of high-quality porous films because of a large number of point defects in the porous structure. The crystallographic approach to control AAO morphology is applicable also for the large-scale anodization using polycrystalline Al foils subjected to a texturizing via rolling and/or annealing.[56,57]

The most pronounced effect of Al crystallography on the AAO morphology has been observed for the samples obtained in sulfuric acid electrolyte. Nevertheless, the structure of anodic alumina films prepared in oxalic acid is also strongly depended on the substrate symmetry. In the case of hard anodization the presence of the inhomogeneous oxide layer in the top part of the porous structure as well as an increase in temperature at the AAO/Al interface due to high current density can eliminate distinctions between the morphology of AAO on single-crystal substrates with different crystallographic orientations. Moreover, current density in the hard anodization process is known to be limited by the diffusion of reagents or products of chemical reaction through the channels of anodic alumina.[21,53] This fact restricts crystallography impact in comparison with mild anodization conditions, where the rate-determining step

DOI: 10.1021/acs.jpcc.7b09998
J. Phys. Chem. C 2017, 121, 27511−27520

Table 1. Ordering Parameters of Porous Oxide Films Formed on Different Low-Index Surfaces of Al Single Crystals under Various Anodization Conditions (25 V in 0.3 M Sulfuric Acid; 40 and 120 V in 0.3 M Oxalic Acid)[a]

	0.3 M sulfuric acid, 25 V				0.3 M oxalic acid, 40 V				0.3 M oxalic acid, 120 V			
	q, C cm^{-2} μm^{-1}	ψ, %	φ, deg.	δq_z, deg.	q, C cm^{-2} μm^{-1}	ψ, %	φ, deg.	δq_z, deg.	q, C cm^{-2} μm^{-1}	ψ, %	φ, deg.	δq_z, deg.
Al(100)	1.95 ± 0.02	90.5 ± 0.9		0.25 ± 0.01	2.47 ± 0.01	90.4 ± 0.5		0.32 ± 0.01	1.90 ± 0.03	85.8 ± 0.6		0.55 ± 0.04
Al(110)	1.90 ± 0.01	79.1 ± 1.1	46.9 ± 0.2	0.33 ± 0.01	2.77 ± 0.01	90.4 ± 0.5	39.2 ± 2.5	0.37 ± 0.02	1.88 ± 0.02	85.5 ± 0.6	48.2 ± 0.5	0.58 ± 0.02
Al(111)	1.77 ± 0.01	86.5 ± 0.6	21.2 ± 0.1	0.31 ± 0.01	2.37 ± 0.02	91.3 ± 0.4	33.7 ± 0.5	0.40 ± 0.01	1.77 ± 0.02	86.2 ± 0.4	42.9 ± 1.7	0.61 ± 0.01

[a]Specific charge values (q), a percentage of pores with a hexagonal coordination environment (ψ), mosaicity according to statistical analysis of SEM images (φ), and FWHM of the rocking curves (δq_z) are present.

for oxide formation is associated with the processes in barrier layer separating aluminum and electrolyte.[21,58]

CONCLUSIONS

Anodic alumina films with highly ordered porous structures were grown on the aluminum single-crystal low-index surfaces in a wide variety of experimental conditions. The kinetics of the anodization process is found to be dependent on the aluminum substrate crystallography and confirm activation character for all anodization conditions. The barrier height difference of 15−20 meV for Al(100) and Al(111) as compared to Al(110) substrates has been ascribed to the energy difference of aluminum atom release from the metal surface to the oxide layer.

The symmetry of the substrate is found to be inherited in the AAO porous structure, with the best in-plane orientational pore ordering achieved on the Al(111) facet, while providing the best longitudinal orientational arrangement (along the pore direction) on the Al(100) substrates. Our findings allow one to precisely adjust the morphology of the AAO porous films via the proper selection of the Al substrate symmetry.

ASSOCIATED CONTENT

Supporting Information

The Supporting Information is available free of charge on the ACS Publications website at DOI: 10.1021/acs.jpcc.7b09998.

Calculation of activation barrier differences and oxidation rate ratio for anodic oxidation of low-index aluminum faces. (PDF)

AUTHOR INFORMATION

Corresponding Author

*E-mail: kirill@inorg.chem.msu.ru. Phone: +7-495-9395248. Fax: +7-495-9390998.

ORCID

Vladimir K. Ivanov: 0000-0003-2343-2140
Andrei V. Petukhov: 0000-0001-9840-6014
Kirill S. Napolskii: 0000-0002-9353-9114

Notes

The authors declare no competing financial interest.

ACKNOWLEDGMENTS

The work is supported by Russian Science Foundation (Grant No. 17-73-10473). We thank the personnel of the DUBBLE beamline for their excellent support during the experiments. The Nederlandse Organisatie voor Wetenschappelijk Onderzoek is thanked for granting the beam time. The authors are grateful to Aleksandra Rosliakova for programming of the color-coding and domain size analysis algorithms.

REFERENCES

(1) Lee, W.; Park, S. J. Porous Anodic Aluminum Oxide: Anodization and Templated Synthesis of Functional Nanostructures. *Chem. Rev. (Washington, DC, U. S.)* **2014**, *114*, 7487−7556.

(2) Diggle, J. W.; Downie, T. C.; Goulding, C. W. Anodic Oxide Films on Aluminum. *Chem. Rev. (Washington, DC, U. S.)* **1969**, *69*, 365−405.

(3) Poinern, G. E. J.; Ali, N.; Fawcett, D. Progress in Nano-Engineered Anodic Aluminum Oxide Membrane Development. *Materials* **2011**, *4*, 487−526.

DOI: 10.1021/acs.jpcc.7b09998
J. Phys. Chem. C 2017, 121, 27511−27520

(4) Md Jani, A. M.; Losic, D.; Voelcker, N. H. Nanoporous Anodic Aluminium Oxide: Advances in Surface Engineering and Emerging Applications. *Prog. Mater. Sci.* **2013**, *58*, 636−704.
(5) Petukhov, D. I.; Eliseev, A. A. Gas Permeation Through Nanoporous Membranes in the Transitional Flow Region. *Nanotechnology* **2016**, *27*, 085707.
(6) Inada, T.; Uno, N.; Kato, T.; Iwamoto, Y. Meso-Porous Alumina Capillary Tube As a Support for High-Temperature Gas Separation Membranes by Novel Pulse Sequential Anodic Oxidation Technique. *J. Mater. Res.* **2005**, *20*, 114−120.
(7) Napolskii, K. S.; Barczuk, P. J.; Vassiliev, S. Y.; Veresov, A. G.; Tsirlina, G. A.; Kulesza, P. J. Templating of Electrodeposited Platinum Group Metals As a Tool to Control Catalytic Activity. *Electrochim. Acta* **2007**, *52*, 7910−7919.
(8) Leontiev, A. P.; Brylev, O. A.; Napolskii, K. S. Arrays of Rhodium Nanowires Based on Anodic Alumina: Preparation and Electrocatalytic Activity for Nitrate Reduction. *Electrochim. Acta* **2015**, *155*, 466−473.
(9) Sun, L.; Hao, Y.; Chien, C. L.; Searson, P. C. Tuning the Properties of Magnetic Nanowires. *IBM J. Res. Dev.* **2005**, *49*, 79−102.
(10) Chumakov, A. P.; Grigoriev, S. V.; Grigoryeva, N. A.; Napolskii, K. S.; Eliseev, A. A.; Roslyakov, I. V.; Okorokov, A. I.; Eckerlebe, H. Magnetic Properties of Cobalt Nanowires: Study by Polarized SANS. *Phys. B (Amsterdam, Neth.)* **2011**, *406*, 2405−2408.
(11) Hnida, K. E.; Bassler, S.; Akinsinde, L.; Gooth, J.; Nielsch, K.; Socha, R. P.; Laszcz, A.; Czerwinski, A.; Sulka, G. D. Tuning the Polarity of Charge Transport in InSb Nanowires Via Heat Treatment. *Nanotechnology* **2015**, *26*, 285701.
(12) Wang, B.; Fei, G. T.; Wang, M.; Kong, M. G.; Zhang, L. D. Preparation of Photonic Crystals Made of Air Pores in Anodic Alumina. *Nanotechnology* **2007**, *18*, 365601.
(13) Su, Y.; Fei, G. T.; Zhang, Y.; Yan, P.; Li, H.; Shang, G. L.; Zhang, L. D. Controllable Preparation of the Ordered Pore Arrays Anodic Alumina With High-Quality Photonic Band Gaps. *Mater. Lett.* **2011**, *65*, 2693−2695.
(14) Lee, W.; Han, H.; Lotnyk, A.; Schubert, M. A.; Senz, S.; Alexe, M.; Hesse, D.; Baik, S.; Gosele, U. Individually Addressable Epitaxial Ferroelectric Nanocapacitor Arrays With Near Tb Inch^{-2} Density. *Nat. Nanotechnol.* **2008**, *3*, 402−407.
(15) Banerjee, P.; Perez, I.; Henn-Lecordier, L.; Lee, S. B.; Rubloff, G. W. Nanotubular Metal-Insulator-Metal Capacitor Arrays for Energy Storage. *Nat. Nanotechnol.* **2009**, *4*, 292−296.
(16) Dickey, C. E.; Varghese, K. O.; Ong, G. K.; Gong, D.; Paulose, M.; Grimes, A. C. Room Temperature Ammonia and Humidity Sensing Using Highly Ordered Nanoporous Alumina Films. *Sensors* **2002**, *2*, 91−110.
(17) Gorokh, G.; Mozalev, A.; Solovei, D.; Khatko, V.; Llobet, E.; Correig, X. Anodic Formation of Low-Aspect-Ratio Porous Alumina Films for Metal-Oxide Sensor Application. *Electrochim. Acta* **2006**, *52*, 1771−1780.
(18) Karpov, E. E.; Karpov, E. F.; Suchkov, A.; Mironov, S.; Baranov, A.; Sleptsov, V.; Calliari, L. Energy Efficient Planar Catalytic Sensor for Methane Measurement. *Sens. Actuators, A* **2013**, *194*, 176−180.
(19) Petukhov, D. I.; Napolskii, K. S.; Berekchiyan, M. V.; Lebedev, A. G.; Eliseev, A. A. Comparative Study of Structure and Permeability of Porous Oxide Films on Aluminum Obtained by Single- and Two-Step Anodization. *ACS Appl. Mater. Interfaces* **2013**, *5*, 7819−7824.
(20) Noyan, A. A.; Leontiev, A. P.; Yakovlev, M. V.; Roslyakov, I. V.; Tsirlina, G. A.; Napolskii, K. S. Electrochemical Growth of Nanowires in Anodic Alumina Templates: The Role of Pore Branching. *Electrochim. Acta* **2017**, *226*, 60−68.
(21) Roslyakov, I. V.; Gordeeva, E. O.; Napolskii, K. S. Role of Electrode Reaction Kinetics in Self-Ordering of Porous Anodic Alumina. *Electrochim. Acta* **2017**, *241*, 362−369.
(22) Grigoriev, S. V.; Grigorieva, N. A.; Syromyatnikova, A. V.; Napolskii, K. S.; Eliseev, A. A.; Lukashin, A. V.; Tret'yakov, Y. D.; Eckerlebe, H. Two-Dimensional Spatially Ordered Al_2O_3 Systems: Small-Angle Neutron Scattering Investigation. *JETP Lett.* **2007**, *85*, 449−453.
(23) Beck, G.; Petrikowski, K. Influence of the Microstructure of the Aluminum Substrate on the Regularity of the Nanopore Arrangement in an Alumina Layer Formed by Anodic Oxidation. *Surf. Coat. Technol.* **2008**, *202*, 5084−5091.
(24) Beck, G.; Bretzler, R. Regularity of Nanopores in Anodic Alumina Formed on Orientated Aluminium Single-Crystals. *Mater. Chem. Phys.* **2011**, *128*, 383−387.
(25) Ng, C. K. Y.; Ngan, A. H. W. Precise Control of Nanohoneycomb Ordering Over Anodic Aluminum Oxide of Square Centimeter Areas. *Chem. Mater.* **2011**, *23*, 5264−5268.
(26) Cheng, C.; Ng, K. Y.; Aluru, N. R.; Ngan, A. H. W. Simulation and Experiment of Substrate Aluminum Grain Orientation Dependent Self-Ordering in Anodic Porous Alumina. *J. Appl. Phys.* **2013**, *113*, 204903.
(27) Napolskii, K. S.; Roslyakov, I. V.; Romanchuk, A. Y.; Kapitanova, O. O.; Mankevich, A. S.; Lebedev, V. A.; Eliseev, A. A. Origin of Long-Range Orientational Pore Ordering in Anodic Films on Aluminium. *J. Mater. Chem.* **2012**, *22*, 11922−11926.
(28) Napolskii, K. S.; Roslyakov, I. V.; Eliseev, A. A.; Petukhov, A. V.; Byelov, D. V.; Grigorieva, N. A.; Bouwman, W. G.; Lukashin, A. V.; Kvashnina, K. O.; Chumakov, A. P.; et al. Long-Range Ordering in Anodic Alumina Films: A Microradian X-ray Diffraction Study. *J. Appl. Crystallogr.* **2010**, *43*, 531−538.
(29) Roslyakov, I. V.; Eliseev, A. A.; Yakovenko, E. V.; Zabelin, A. V.; Napolskii, K. S. Longitudinal Pore Alignment in Anodic Alumina Films Grown on Polycrystalline Metal Substrates. *J. Appl. Crystallogr.* **2013**, *46*, 1705−1710.
(30) Roslyakov, I. V.; Koshkodaev, D. S.; Eliseev, A. A.; Hermida-Merino, D.; Petukhov, A. V.; Napolskii, K. S. Crystallography-Induced Correlations in Pore Ordering of Anodic Alumina Films. *J. Phys. Chem. C* **2016**, *120*, 19698−19704.
(31) Mescrel: Metal Single Crystals, Single Crystal Electrodes and Substrates. http://www.mescrel.com/en/; accessed Nov 17, 2017.
(32) Masuda, H.; Satoh, M. Fabrication of Gold Nanodot Array Using Anodic Porous Alumina As an Evaporation Mask. *Jpn. J. Appl. Phys.* **1996**, *35*, L126−L129.
(33) Bras, W.; Dolbnya, I. P.; Detollenaere, D.; van Tol, R.; Malfois, M.; Greaves, G. N.; Ryan, A. J.; Heeley, E. Recent Experiments on a Small-Angle/Wide-Angle X-ray Scattering Beam Line at the ESRF. *J. Appl. Crystallogr.* **2003**, *36*, 791−794.
(34) Petukhov, A. V.; Thijssen, J. H. J.; 't Hart, D. C.; Imhof, A.; van Blaaderen, A.; Dolbnya, I. P.; Snigirev, A.; Moussaid, A.; Snigireva, I. Microradian X-ray Diffraction in Colloidal Photonic Crystals. *J. Appl. Crystallogr.* **2006**, *39*, 137−144.
(35) Thijssen, J. H. J.; Petukhov, A. V.; 't Hart, D. C.; Imhof, A.; van der Werf, C. H. M.; Schropp, R. E. I.; van Blaaderen, A. Characterization of Photonic Colloidal Single Crystals by Microradian X-ray Diffraction. *Adv. Mater.* **2006**, *18*, 1662−1666.
(36) Petukhov, A. V.; Meijer, J. M.; Vroege, G. J. Particle Shape Effects in Colloidal Crystals and Colloidal Liquid Crystals: Small-Angle X-ray Scattering Studies With Microradian Resolution. *Curr. Opin. Colloid Interface Sci.* **2015**, *20*, 272−281.
(37) Snigirev, A.; Kohn, V.; Snigireva, I.; Lengeler, B. A Compound Refractive Lens for Focusing High-Energy X-rays. *Nature* **1996**, *384*, 49−51.
(38) Bosak, A.; Snigireva, I.; Napolskii, K. S.; Snigirev, A. High-Resolution Transmission X-ray Microscopy: A New Tool for Mesoscopic Materials. *Adv. Mater.* **2010**, *22*, 3256−3259.
(39) Hillebrand, R.; Muller, F.; Schwirn, K.; Lee, W.; Steinhart, M. Quantitative Analysis of the Grain Morphology in Self-Assembled Hexagonal Lattices. *ACS Nano* **2008**, *2*, 913−920.
(40) Aurenhammer, F.; Klein, R. Voronoi Diagrams. In *Handbook of Computational Geometry*; Sack, J.-R., Urrutia, J., Eds.; North-Holland: Amsterdam, 2000; Vol. 5, pp 201−290.
(41) Schneider, C. A.; Rasband, W. S.; Eliceiri, K. W. NIH Image to ImageJ: 25 Years of Image Analysis. *Nat. Methods* **2012**, *9*, 671−675.
(42) Software for Analysis of Pore Ordering in Anodic Alumina. http://www.eng.fnm.msu.ru/software/; accessed Nov 17, 2017.

DOI: 10.1021/acs.jpcc.7b09998
J. Phys. Chem. C 2017, 121, 27511−27520

(43) Hartman, P.; Perdok, W. G. On the Relations Between Structure and Morphology of Crystals I. *Acta Crystallogr.* **1955**, *8*, 49−52.
(44) Sangwal, K. *Etching of Crystals: Theory, Experiment, and Application*; North-Holland: Amsterdam, 1987.
(45) Vetter, K. J. *Electrochemical Kinetics: Theoretical and Experimental Aspects*; Academic Press: New York, 1967.
(46) Stedman, R.; Nilsson, G. Dispersion Relations for Phonons in Aluminum at 80 and 300 K. *Phys. Rev.* **1966**, *145*, 492−500.
(47) Eguchi, S. Anodic Oxide Films on Aluminum Formed in Oxalic Acid, Orthophosphoric Acid, and Chromic Acid Solutions Studies on Anodic Oxidation of Aluminum (Part 5). *Kinzoku Hyomen Gijutsu* **1969**, *20*, 493−499.
(48) Patermarakis, G.; Lenas, P.; Karavassilis, C.; Papayiannis, G. Kinetics of Growth of Porous Anodic Al_2O_3 Films on Al Metal. *Electrochim. Acta* **1991**, *36*, 709−725.
(49) Parkhutik, V. P.; et al. Theoretical Modelling of Porous Oxide Growth on Aluminium. *J. Phys. D: Appl. Phys.* **1992**, *25*, 1258−1263.
(50) Kim, M.; Kim, H.; Bae, C.; Lee, J.; Yoo, H.; Moreno, J. M. M.; Shin, H. Initial Self-Ordering of Porous Anodic Alumina: Transition From Polydispersity to Monodispersity. *J. Phys. Chem. C* **2014**, *118*, 26789−26795.
(51) Crawford, G. A.; Chawla, N. Tailoring TiO_2 Nanotube Growth During Anodic Oxidation by Crystallographic Orientation of Ti. *Scr. Mater.* **2009**, *60*, 874−877.
(52) Roslyakov, I. V.; Kuratova, N. S.; Koshkodaev, D. S.; Merino, D. H.; Lukashin, A. V.; Napolskii, K. S. Morphology of Anodic Alumina Films Obtained by Hard Anodization: Influence of the Rate of Anodization Voltage Increase. *J. Surf. Invest.: X-Ray, Synchrotron Neutron Tech.* **2016**, *10*, 191−197.
(53) Vega, V.; Garcia, J.; Montero-Moreno, J. M.; Hernando, B.; Bachmann, J.; Prida, V. M.; Nielsch, K. Unveiling the Hard Anodization Regime of Aluminum: Insight into Nanopores Self-Organization and Growth Mechanism. *ACS Appl. Mater. Interfaces* **2015**, *7*, 28682−28692.
(54) Han, G.; Chen, Y.; He, B. Blind Reconstruction of Atomic Force Microscopy Tip Morphology by Using Porous Anodic Alumina Membrane. *Micro Nano Lett.* **2012**, *7*, 1282−1284.
(55) Dremov, V.; Fedoseev, V.; Fedorov, P.; Grebenko, A. Simple and Reliable Method of Conductive SPM Probe Fabrication Using Carbon Nanotubes. *ArXiv:1406.5117v2.*
(56) Engler, O.; Huh, M.-Y. Evolution of the Cube Texture in High Purity Aluminum Capacitor Foils by Continuous Recrystallization and Subsequent Grain Growth. *Mater. Sci. Eng., A* **1999**, *271*, 371−381.
(57) Kobayashi, M.; Takayama, Y.; Kato, H. Preferential Growth of Cube-Oriented Grains in Partially Annealed and Additionally Rolled Aluminum Foils for Capacitors. *Mater. Trans.* **2004**, *45*, 3247−3255.
(58) Curioni, M.; Koroleva, E. V.; Skeldon, P.; Thompson, G. E. Flow Modulated Ionic Migration During Porous Oxide Growth on Aluminium. *Electrochim. Acta* **2010**, *55*, 7044−7049.

DOI: 10.1021/acs.jpcc.7b09998
J. Phys. Chem. C 2017, 121, 27511−27520